A Novel Microstrip Square-Loop Dual-Mode Bandpass Filter With Simultaneous Size Reduction and Spurious Response Suppression

Si-Weng Fok, *Student Member, IEEE*, Pedro Cheong, *Member, IEEE*, Kam-Weng Tam, *Senior Member, IEEE*, and Rui P. Martins, *Senior Member, IEEE*

***Abstract*—In this paper, a new capacitively stepped-impedance resonator (CSIR) is proposed to develop the microstrip square-loop dual-mode bandpass filter. Using this new design, simultaneous size reduction and spurious response suppression for the dual-mode bandpass filter can be achieved. An analytical formulation of this novel resonator is given in order to elucidate the spurious frequencies relocation design. Together with this formulation, a generalized dual-mode bandpass filter model is developed so as to ease the analysis of transmission zero and insertion loss. A prototype filter is designed at 900 MHz with 1.5% fractional bandwidth. Significant spurious suppressions up to 33 and 35 dB are measured at 1.8 and at 2.7 GHz, respectively. A circuitry size reduction of 54% is achieved when compared with that of the conventional structure. Moreover, the CSIR allows frequency tuning and, thus, a varactor-tuned filter is designed and a measured tunable center frequency between 1.5–1.62 GHz is demonstrated. Utilizing the proposed structure, not only size reduction, as well as spurious response suppression, but also center frequency tuning can be achieved.**

***Index Terms*—Dual-mode resonator, insertion loss, size reduction, spurious response suppression.**

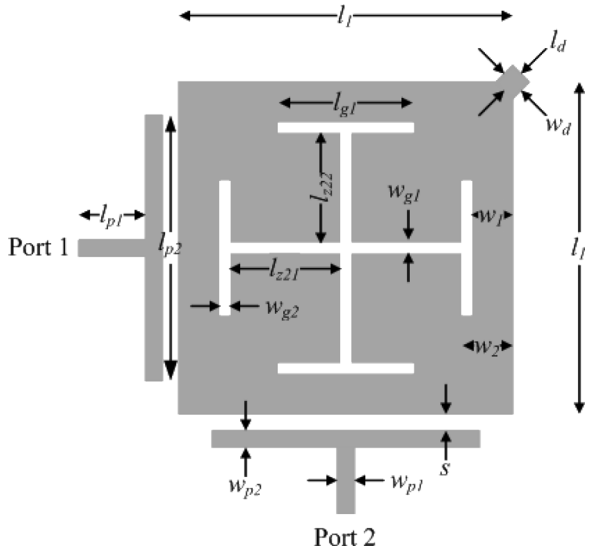

Fig. 1. Microstrip dual-mode bandpass filter using CSIR.

I. Introduction

A VARIETY of microstrip dual-mode bandpass filters have been proposed over the past decade [1]–[5]. The filter compactness and selectivity improvement are the recent research focuses. The dual-mode bandpass filter using a square-loop resonator has achieved circuitry size reduction through the capacitive loaded arms and transmission zeros can be also easily introduced in the passband proximity to improve the filter selectivity [5]–[9]. However, this filter may suffer from the problem of spurious responses and these responses are located at the harmonic frequencies of the fundamental frequency. This indeed degrades the stopband rejection and becomes an intrinsic performance limitation associated with wide stopband applications. Thus, the systematic dual-mode bandpass filter design that is able to simultaneously realize both spurious responses suppression, as well as size reduction, is required. Moreover, the passband insertion loss is normally in excess and its relationship with the input/output port coupling is concerned.

Manuscript received October 7, 2005; revised February 20, 2006. This work was supported by the Research Committee of the University of Macau under Research Project RG009/04-05S/C62/MR/FST.

The authors are with the Wireless Communication Laboratory, University of Macau, Taipa, Macao SAR, China (e-mail: kentam@umac.mo).

Digital Object Identifier 10.1109/TMTT.2006.873626

A simple and compact dual-mode square-loop resonator bandpass filter using capacitively stepped-impedance resonator (CSIR), as depicted in Fig. 1, has been proposed [10]. This CSIR is used to develop the square-loop resonator. It is modeled as a SIR transmission line together with a loading capacitor midway along the transmission line. Significant improvement in first and second spurious responses suppression, as well as filter size miniaturization, is realized under this new topology. In this paper, an analytical discussion of the spurious responses suppression and size minimization capabilities of the proposed dual-mode filter topology will be outlined. Moreover, the formulation of the two transmission zeros lying on either side of the passband is presented and an estimation of the loss induced by the input/output coupling ports is also derived.

Besides this introduction, there are four additional sections. The novel dual-mode bandpass filter structure takes full advantage of the proposed CSIR to relocate the unwanted spurious to higher frequency range and to reduce circuitry size. These intrinsic characteristics are discussed in Section II. In Section III, a transmission model of the dual-mode filter is derived and this model is adopted in the passband modeling and transmission zeros calculation. A derivation on the passband insertion loss influenced by the input/output coupling ports is proposed. To demonstrate the filter's performance, design examples are given in Section IV and, finally, a conclusion is drawn in Section V.

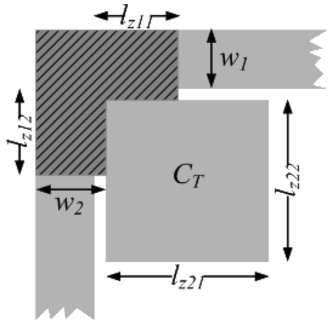

Fig. 2. One-quarter of the square-loop resonator of Fig. 1.

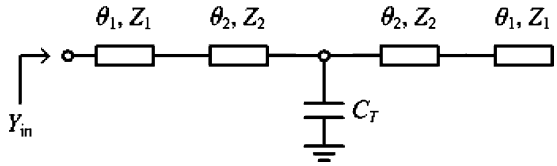

Fig. 3. Composite transmission-line model of Fig. 2.

II. Spurious Response Suppression and Size Reduction of CSIR

The use of a capacitive arm to reduce the size of the microstrip square-loop dual-mode bandpass filter has been demonstrated and different capacitive arms have also been proposed over the years [8], [9]. This arm is usually attached to the square-loop resonator inner corner. Even the analysis is not trivial, a complex pattern is introduced to increase the loading capacitance for size reduction. In order to analytically formulate the capacitive arm effect on the dual-mode filter, a simple CSIR structure is proposed and its application for the filter's spurious response suppression discussion is also studied [10]. One-quarter of the square-loop resonator based on the CSIR is considered as shown in Fig. 2. The introduction of the capacitive loading C_T attached to a square-loop resonator is simply a rectangle patch with lengths l_{z21} and l_{z22}. A stepped-impedance configuration is applied on the conventional square-loop resonator and its low-impedance portions are with different lengths l_{z11} and l_{z12}. When this CSIR is used for the dual-mode bandpass filter, it is observed that proper control of these parameters can distance a filter's spurious frequencies and reduce its circuitry size simultaneously [10].

A. Spurious-Response Suppression

By modeling the proposed CSIR as a composite transmission line with loading capacitance C_T inserted midway on the two line segments and open-end termination, as shown in Fig. 3, distinct characteristic impedances ($Z_1 \neq Z_2$) and electrical lengths ($\theta_1 \neq \theta_2$) are assumed. In fact, ignoring the influences of a step discontinuity in Fig. 3 and its admittance Y_{in} can be derived as follows:

$$Y_{\text{in}} = \frac{-j\left(\varphi_1 \times (\varphi_2 - \varphi_3)\right)}{Z_1(\cos\theta_1 \sin\theta_1(\omega C_T Z_1^2 Z_2 \cos^2\theta_2 - \sin\theta_2 \times \varphi_4) + \varphi_5 - \varphi_6)} \quad (1)$$

where

$$\begin{aligned}
\varphi_1 &= Z_1 \cos\theta_1 \cos\theta_2 - Z_2 \sin\theta_1 \sin\theta_2 \\
\varphi_2 &= Z_1 \cos\theta_1(\omega C_T Z_2 \cos\theta_2 - 2\sin\theta_2) \\
\varphi_3 &= Z_2 \sin\theta_1(2\cos\theta_2 + \omega C_T Z_2 \sin\theta_2) \\
\varphi_4 &= 2\left(Z_1^2 + Z_2^2\right)\cos\theta_2 + \omega C_T Z_2^3 \sin\theta_2 \\
\varphi_5 &= \frac{1}{2} Z_1 Z_2 \cos^2\theta_1 \left[2\cos(2\theta_2) + \omega C_T Z_2 \sin(2\theta_2)\right] \\
\varphi_6 &= \frac{1}{2} Z_1 Z_2 \sin^2\theta_1 \left[2\cos(2\theta_2) + \omega C_T Z_2 \sin(2\theta_2)\right].
\end{aligned}$$

From (1), the resonance conditions occur when $Y_{\text{in}} = \infty$ and 0. By solving these conditions, the different resonance modes can be described by

$$f_{4k} - \text{mode}: \ 2\theta_1 + \gamma = 2k\pi \quad (2a)$$
$$f_{4k+1} \text{ mode}: \ \cot\theta_2 = K\tan\theta_1 \quad (2b)$$
$$f_{4k+2} \text{ mode}: \ 2\theta_1 + \gamma = (2k+1)\pi \quad (2c)$$
$$f_{4k+3} \text{ mode}: \ \cot(\theta_2 - \alpha) = K\tan\theta_1 \quad (2d)$$

where

$$\begin{aligned}
&k = 0, 1, 2, \ldots \\
&\alpha = \tan^{-1}\left(\frac{2}{\omega Z_2 C_T}\right) \\
&\gamma = \tan^{-1}\left(\frac{2Z_1 Z_2 \sin(2\theta_2 - \alpha)}{(Z_1^2 + Z_2^2)\cos(2\theta_2 - \alpha) + (Z_1^2 - Z_2^2)\cos\alpha}\right) \\
&K = Z_2/Z_1.
\end{aligned}$$

By solving (2), the fundamental (f_0) and spurious frequencies (first, second, third, and fourth spurious resonances, e.g., f_1, f_2, f_3, and f_4) can then be determined using a simple root-searching program. The resonator becomes a uniform impedance transmission when either θ_1 or θ_2 is zero. For a CSIR designed at $f_0 = 900$ MHz on a substrate RO4003 with $\varepsilon_r = 3.38$ and $h = 1.524$ mm, Figs. 4 and 5 show the characteristics of the first, second, third, and fourth spurious frequencies normalized to their fundamental frequency against the normalized electrical length $\theta_1/(\theta_1 + \theta_2)$. Fig. 4 is plotted for different loading capacitances ($C_T = 2, 3$, and 4 pF) subject to $K = 0.86$ as the impedance ratio; an increase in the loading capacitance distances the spurious frequencies to higher frequency band, grouping f_1, f_2, and f_3 more closely to one another. If equal electrical lengths are assumed to ease the filter design, the first to fourth spurious frequencies relocate to $3.0f_0$, $3.5f_0$, $3.9f_0$, and $6.0f_0$, respectively, when 4-pF loading capacitance is considered. On the other hand, the impedance ratio K is varied from 0.68 to 1.20, and its effect on the CSIR is studied in Fig. 5. For a loading capacitance of 2 pF, a smaller K could be beneficial for all spurious frequency relocation within a specific range of electrical lengths.

B. Size Reduction

As illustrated in Fig. 6, the CSIR discussed in Section II-A is further investigated when the loading capacitance C_T is varied from 0 to 10 pF and the impedance ratio is fixed at 0.86. It is obvious that increasing the loading capacitance will distance

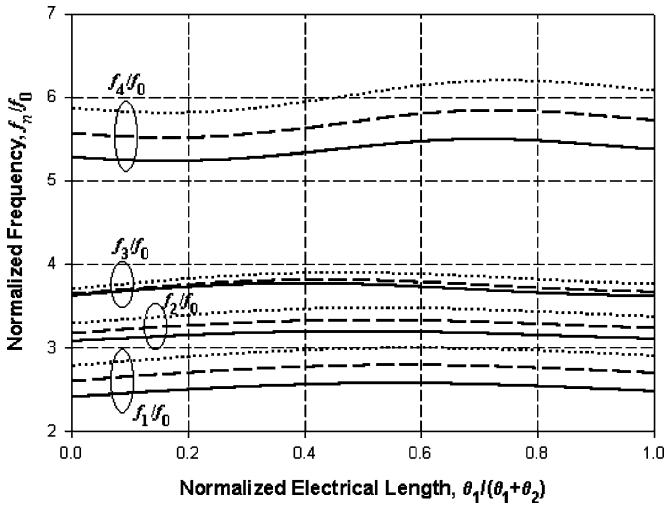

Fig. 4. Ratio of first, second, third, and fourth spurious frequencies to the fundamental frequency of CSIR for $K = 0.86$(— : $C_T = 2$ pF; – – : $C_T = 3$ pF; ··· : $C_T = 4$ pF).

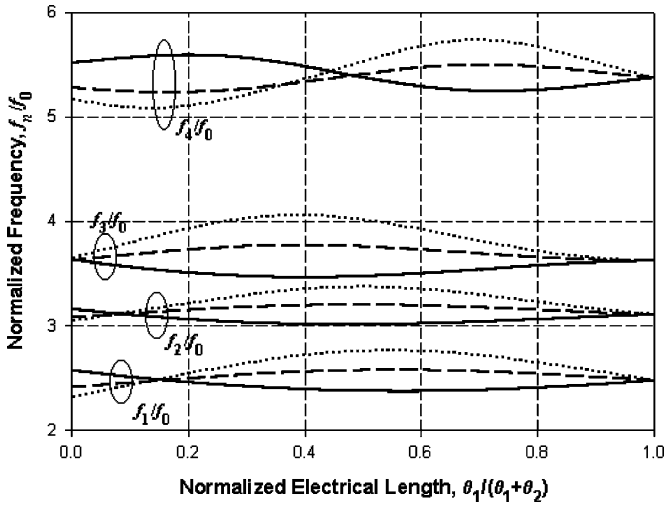

Fig. 5. Ratio of first, second, third, and fourth spurious frequencies to the fundamental frequency of CSIR for $C_T = 2$ pF (··· : $K = 0.68$; – – : $K = 0.86$; — : $K = 1.20$).

the fundamental frequency to a lower frequency band; thus implying that a bandpass response at a lower frequency could be designed by higher frequency parameters with the introduction of loading capacitance. This is indeed the main property accounting for size reduction. In fact, the normalized resonator length L_n of the CSIR is expressed as

$$L_n = \frac{2(\theta_1+\theta_2)}{\pi/2} = \frac{2\left(-\gamma/2+\theta_2\right)}{\pi/2}. \tag{3}$$

For some values of K and θ_2, a larger C_T reduces L_n. The normalized length reduction in the arm, denoted as ΔL_n, is plotted against different loading capacitances, as shown in Fig. 6, and

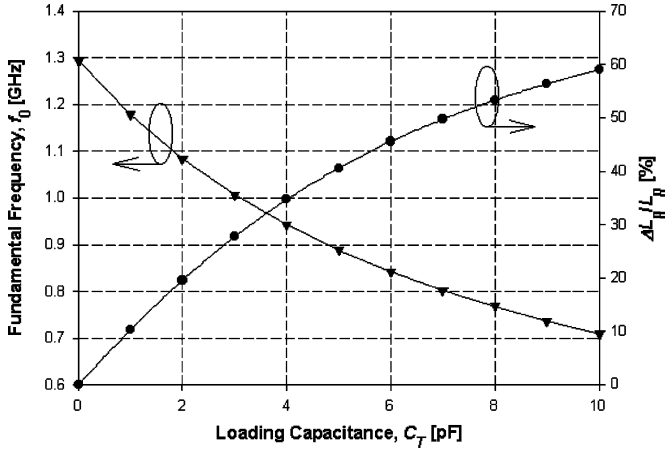

Fig. 6. Normalized fundamental frequency and length reduction ΔL_n against C_T.

approximately 40% electrical length reduction is yielded when a 4.8-pF capacitance is used.

III. Analysis of Microstrip Square-Loop Dual-Mode Bandpass Filter Using CSIR

A. Transmission Zeros

A simple transmission-line model is elaborated to explore the transmission zero of the microstrip square-loop dual-mode bandpass filter using the proposed CSIR. Its overall equivalent circuit is shown in Fig. 7. Acting as a shunt circuit, this loop resonator can be divided into upper and lower parts between the input and output ports. The upper one is made up of the three CSIRs CSIR_1, CSIR_2, and CSIR_3, whereas the lower part has only a single element CSIR_4. To account for the right-angle effect, the CSIR in Fig. 3 is now added with the equivalent circuit of 90° right-angle bend that is modeled by a T-network with inductor L_{bend} and capacitor C_{bend} and their expressions are given in [11]. In CSIR_2, there are two extra capacitances C_s and C_{oc} in parallel with C_T, as highlighted in Fig. 7. The capacitance C_s models the stub perturbing outwards, as shown in Fig. 1, and the capacitance C_{oc} accounts for the open-end effect introduced by the open stub. The π-capacitance network with coupling gap capacitance C_g and parallel-plate capacitance C_p models input and output ports, respectively.

For spurious response suppression and size reduction, the impedance ratio K of these CSIRs is designed around unity, as addressed in Section II. Similar to [5], the filter's total transfer admittance can thus be determined by calculating $ABCD$- and Y-parameters of the above equivalent circuit. For lower microwave frequencies, the above T-network effect is insignificant. Assume $\theta_1 \approx \theta_2 = \theta$ and $Z_1 \approx Z_2 = Z$, the filter transmission zero is similar to the formulation in [5]

$$Y_{21}^{T} = \frac{1}{Z_{21}^{U}} + \frac{1}{Z_{21}^{L}} \tag{4}$$

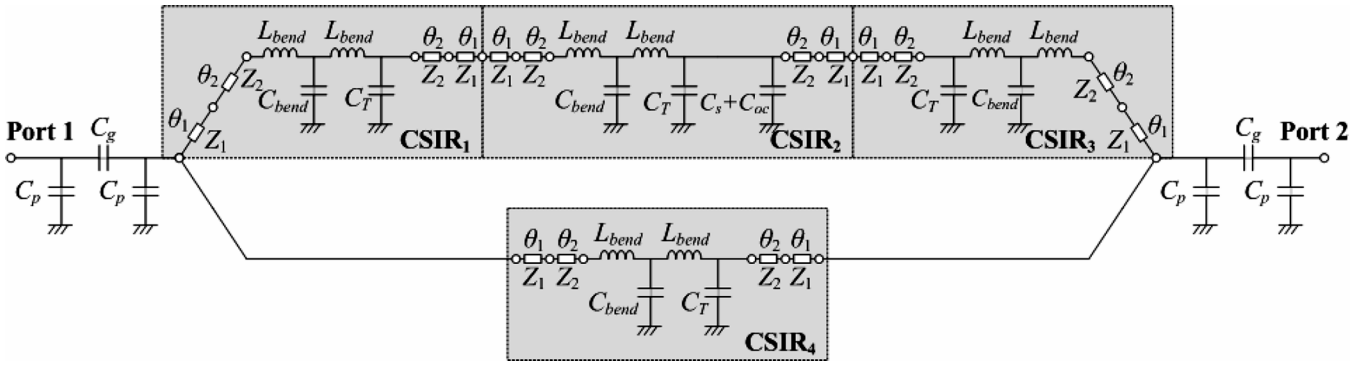

Fig. 7. Equivalent circuit of the dual-mode bandpass filter using CSIR.

TABLE I
ELEMENT VALUES USED IN THE EQUIVALENT CIRCUIT OF AN EXAMPLE 900-MHZ BANDPASS FILTER

C_g	C_p	l'_1	l'_2	L_{bend}
0.6 pF	0.01 pF	8.85 mm	7.35 mm	0.15 pH
C_{bend}	C_T	C_s	C_{oc}	
6.87 fF	4.8 pF	0.53 fF	44.6 fF	

where

$$Z_{21}^{U} = j\frac{1}{2}Z\sin(2\theta)\alpha_1\left[-4\cos(6\theta)+2\omega Z\sin(2\theta)\alpha_2\right]$$
$$Z_{21}^{L} = -jZ\sin(2\theta)\left[-2\cos(2\theta)+\omega C_T Z\sin(2\theta)\right]$$
$$\alpha_1 = -1-2\cos(4\theta)+\omega C_T Z\sin(4\theta)$$
$$\alpha_2 = C_s+C_T+2(C_s+2C_T)\cos(4\theta) - \omega C_T(C_s+C_T)Z\sin(4\theta).$$

Based on the above transmission-line model, an example dual-mode bandpass filter is designed at 900 MHz on a substrate RO4003 with $\varepsilon_r = 3.38$ and $h = 1.524$ mm and the corresponding element values are summarized in Table I. The electrical length $\theta_{1,2}$ is equivalent to $\beta_{1,2}l'_{1,2}$, where $l'_{1,2}$ are the physical lengths employed in the example filter. Its calculated transfer characteristic is plotted against the simulated ones [12], as depicted in Fig. 8. Good agreement between these two responses is observed to validate the proposed filter model correctness. Two calculated transmission zeros (lower transmission zero f_{z1} and upper transmission zero f_{z2}) of the above bandpass filter example are recorded at 0.885 and 0.938 GHz, respectively. Only 15- and 6-MHz frequency derivations are observed between the calculated and simulated results. To explore the capacitive load effect on these zeros, Fig. 9 records the values of these two transmission zeros against some loading capacitances based on (4). The calculated zeros are also plotted against the simulation results [12]. Their maximum deviation is only 25 MHz and it is found that the separation of these two zeros remains almost constant as C_T changes.

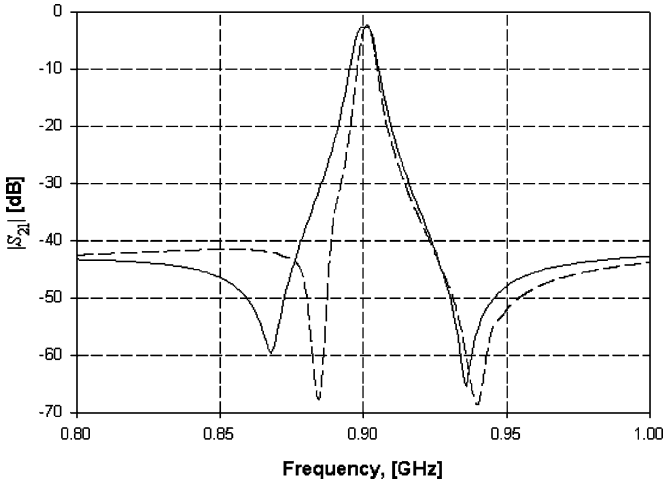

Fig. 8. Transfer characteristics of proposed dual-mode bandpass filter (——: simulated; – – –: calculated).

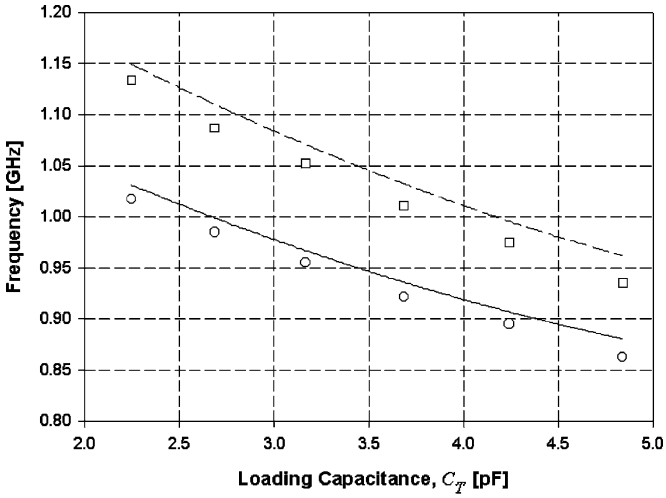

Fig. 9. Transmission zeros location of the proposed dual-mode bandpas filter against C_T ("○": calculated f_{z1}; "□": calculated f_{z2}; ——: simulated f_{z1}; – – –: simulated f_{z2}).

B. Passband Insertion Loss

For the above example filter, the calculated passband insertion loss is 2.4 dB, whereas the simulated value is 2.7 dB, as shown in Fig. 10. On the other hand, the calculated center frequency is at 902 MHz with a 3-dB bandwidth of 4.3 MHz, while the simulated value has a 3-dB bandwidth of 7 MHz and its

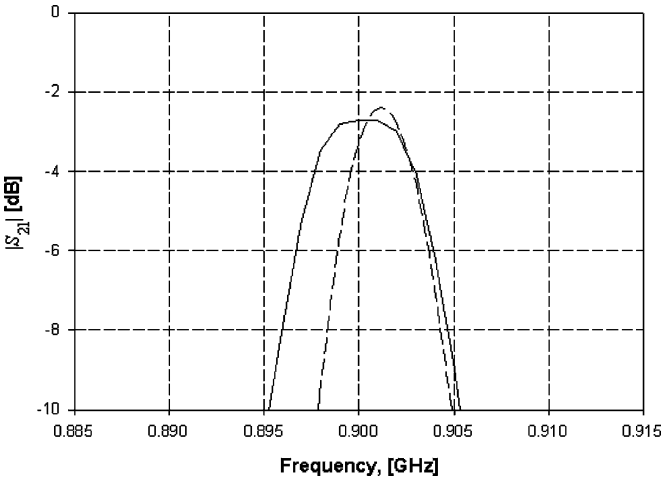

Fig. 10. Passband insertion loss of proposed dual-mode bandpass filter (——: simulated; – – –: calculated).

center frequency is at 900 MHz. This difference is due to our simplified modeling of line-to-ring coupling.

As the dual-mode filter's passband insertion loss severely depends on the gap distance between the port and the ring resonator [13], an inverter model is employed to replace the capacitive π-network so as to ease the analysis. For dual-mode structure, the ring resonator exhibits shunt-type resonance, thus, the J-inverter will be used instead of the K-inverter with the expressions for the J-inverter given by [14]

$$J = Y_0 \left| \tan\left(\frac{\phi}{2} + \tan^{-1} \frac{\omega C_p}{Y_0} \right) \right| \tag{5}$$

where

$$\phi = -\tan^{-1}\left(\frac{2\omega C_g}{Y_0} + \frac{\omega C_p}{Y_0} \right) - \tan -1 \frac{\omega C_p}{Y_0}$$

$$Y_0 = \frac{1}{Z_0}$$

and Z_0 is the characteristic impedance of the port.

The proposed dual-mode filter structure can thus be described in a generalized circuit of a doubly loaded single resonator [14], as depicted in Fig. 11. J_i is the J-inverter representing the capacitive π-network between the port and the ring resonator where $i = 1, 2$. The external quality factor Q_{ei} is defined as the quality factor when the resonator is loaded only by Z_0 on the port. In our case, the equal J-inverter is assumed implying $Q_{e1} = Q_{e2} = Q_e$. The unloaded quality factor Q_u of the resonator is its quality factor when both Z_0 terminations are removed and the loss is only contributed by the internal loss of the resonator.

For the resonator shown in Fig. 11, the loaded Q factor Q_L can be given as

$$Q_L = \frac{1}{\frac{1}{Q_{e1}} + \frac{1}{Q_u} + \frac{1}{Q_{e2}}} = \frac{1}{\frac{2}{Q_e} + \frac{1}{Q_u}}. \tag{6}$$

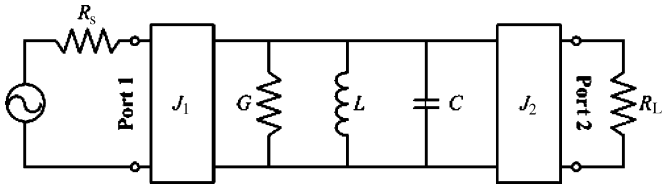

Fig. 11. Doubly loaded single resonator.

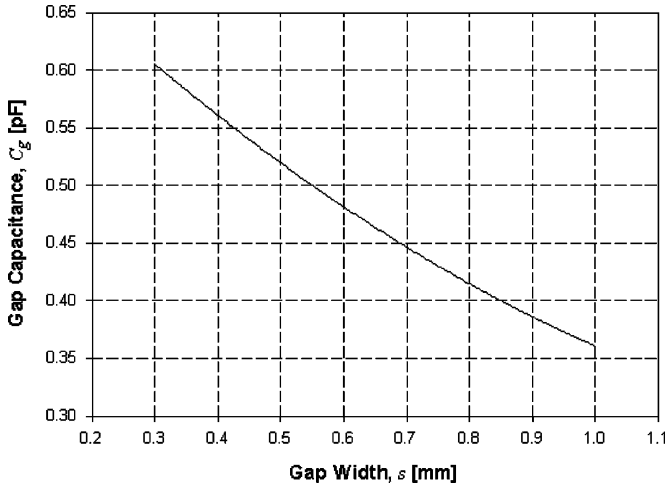

Fig. 12. Equivalent capacitance values of C_g against gapwidth s.

Utilizing the J-inverter value found in (5), the external Q-factor Q_e can be expressed as [14]

$$Q_e = \frac{b}{J^2/Y_0} \tag{7}$$

where b is the susceptance slope parameter

Utilizing (6) and (7), the attenuation through the resonator at resonance can be obtained by

$$L_A = 10 \log_{10} \left(\frac{Q_{e1} Q_{e2}}{4 Q_L^2} \right). \tag{8}$$

To validate (8), L_A is calculated for different port coupling capacitance C_g and is compared with the simulated values. The variation of coupling capacitance C_g is realized by a gapwidth s change. The effect of different gapwidth s on the capacitance C_g is illustrated in Fig. 12. It is obvious that an increase in s leads to a weaker coupling and a decrease in C_g. It is also found that the change in s has only a very slight effect on parallel-plate capacitance C_p. By interpolation, the susceptance slope parameter b is found to be 3.1368×10^{-10} and Q_u is 250. The calculated result of the insertion loss L_A against some gap capacitances shows good agreement with the simulation, as shown in Fig. 13. The above result has shown that decreasing the gap distance will increase the coupling capacitance and, thus, reduce the insertion loss.

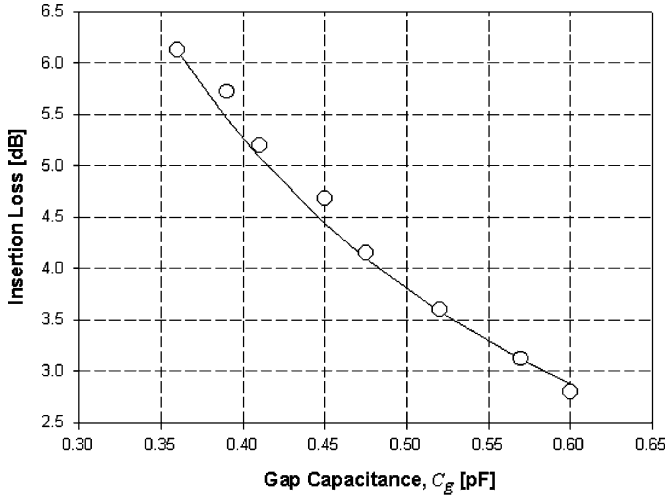

Fig. 13. Insertion loss variation against the gap capacitance C_g (——: calculated; "∘": simulated).

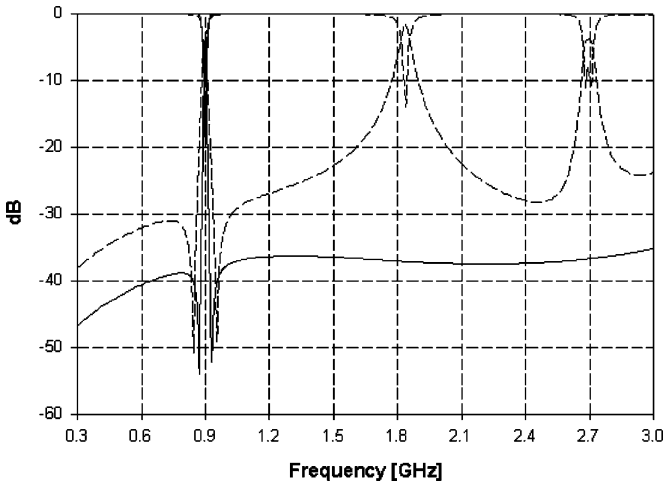

Fig. 14. Comparison of simulated $|S_{11}|$ and $|S_{21}|$ responses of conventional and proposed dual-mode bandpass filters (– – –: conventional; ——: proposed).

TABLE II
DIMENSIONS OF THE EXAMPLE DUAL-MODE FILTER (IN MILLIMETERS)

l_{p1}	l_{p2}	$w_{p1,2}$	s	l_1	w_1
10.00	37.12	2.00	0.30	37.12	2.00
w_2	l_{g1}	$l_{z21,z22}$	$w_{g1,2}$	l_d	w_d
3.00	15.70	15.06	1.00	2.16	2.12

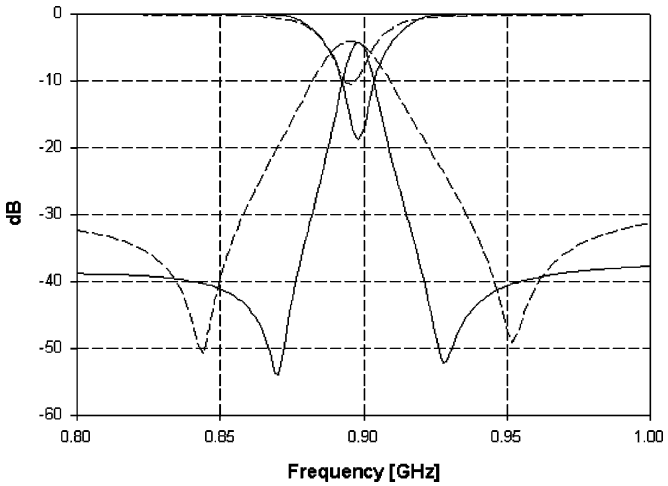

Fig. 15. Comparison of simulated passband $|S_{11}|$ and $|S_{21}|$ responses of conventional and proposed dual-mode bandpass filters (– – –: conventional; ——: proposed).

IV. DESIGN EXAMPLES

A. Microstrip Dual-Mode Bandpass Filter With Simultaneous Size Reduction and Spurious-Responses Suppression

According to the analysis in Section II, it is observed that a smaller K ratio will be more beneficial in spurious-response suppression and size reduction. An example filter at 900 MHz is designed on the substrate RO4003 with a relative dielectric constant of $\varepsilon_r = 3.38$ and thickness $h = 1.524$ mm. Its physical dimensions are summarized in Table II. An identical CSIR is applied onto each side of the square-loop resonator. The width w_1 and w_2 of the CSIR arm is 2 and 3 mm, respectively; thus leading to the impedance ratio K of 0.67. The capacitive loading C_T dimension is 15.06 × 15.06 mm^2, equivalent to a capacitance of 4.5 pF. The circuitry size is only 37.12 × 37.12 mm^2 and around 54% size reduction is achieved by this prototype when compared with the conventional dual-mode filter without an inner CSIR arm. Against the example in [10], an additional 14% size reduction is yielded.

Fig. 14 compares the simulated results of the proposed filter with the conventional structure. Obviously, a wide stopband performance for the proposed dual-mode bandpass filter is reported. Approximately 37-dB suppressions are recorded at the first and second spurious frequencies (1.8 and 2.7 GHz), respectively, leading to the stopband performance with more than 37-dB suppression until three times its fundamental frequency. The passband characteristics of these two filters are also compared in Fig. 15 and it is obvious that the proposed filter offers much selective performance than that of the conventional filter. The simulated 3-dB bandwidth of the new filter is reduced to around 9 MHz; yielding a 1% fractional bandwidth. Two transmission zeros at 0.870 and 0.928 GHz are relocated closer to the passband edges. The insertion loss is 4.3 dB and the matching is kept as good as 19 dB.

This novel dual-mode bandpass filter is also fabricated on the same substrate. The experimental results agree well with the simulation, as shown in Fig. 16. The measured spurious response suppression at 1.8 GHz is around 33 dB, while 35-dB suppression at 2.7 GHz is observed. From Fig. 17, a slight frequency shift of 2 MHz is reported between the simulation and measurement. The measured center frequency is recorded at 902 MHz and the fractional bandwidth is recorded as 1.5%. The upper and lower transmission zeros deviate to 0.876 and 0.944 GHz, respectively. The matching is kept as good as 18 dB and the minimum insertion loss is measured as 4.46 dB. This may be due to the fabrication tolerance in the gapwidth. The photograph of the fabricated filter is presented in Fig. 18(a).

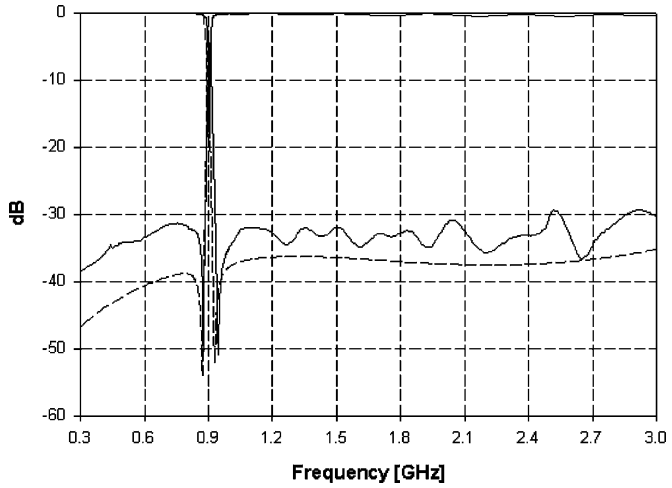

Fig. 16. Comparison of simulated and measured $|S_{11}|$ and $|S_{21}|$ responses of the proposed dual-mode filter (– – –: simulated; ——: measured).

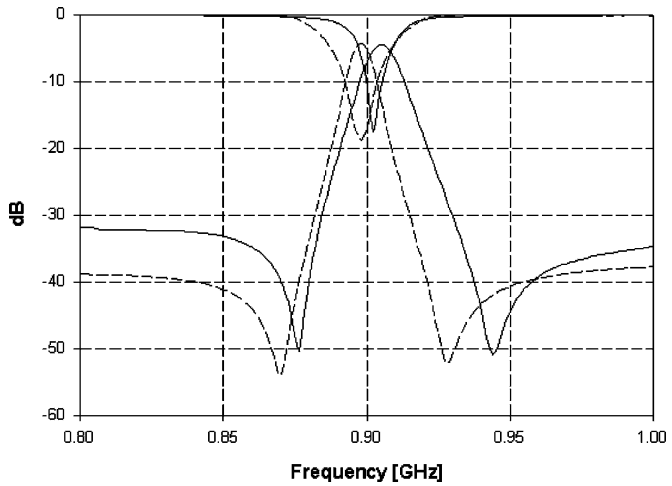

Fig. 17. Comparison of simulated and measured passband $|S_{11}|$ and $|S_{21}|$ responses of the proposed dual-mode filter (– – –: simulated; ——: measured).

B. Varactor-Tuned Microstrip Dual-Mode Bandpass Filter

To demonstrate the frequency-tuning advantage due to the loading capacitance, as shown in Fig. 6, a tunable bandpass filter is also designed. The prototype tunable filter is shown in Fig. 18(b). Its physical dimensions are recorded in Table III. The width w_1 and w_2 of the CSIR arm is 4 and 6 mm, respectively, and the loading capacitance of each CSIR arm is replaced by varactor capacitance C_v. The varactor diode used in the center frequency tuning design is an Infineon BB888 RF variable capacitance diode with a junction capacitance from 0.6 to 10 pF over a 30-V bias voltage. In addition, a series resistance of approximately 1.8 Ω is associated with this diode at a low bias voltage level.

As shown in Fig. 18(b), four varactors are used and equally biased. The measured center frequency tunability of the constructed filter prototype is plotted against the simulations, as shown in Figs. 19 and 20. Good agreement is observed between the experimental and simulated results. Obviously, an overall

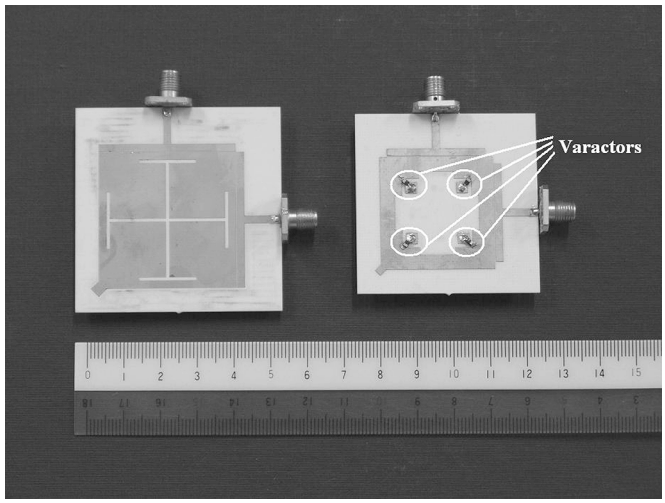

Fig. 18. Photographs of the: (a) compact dual-mode filter prototype and (b) varactor-tuned dual-mode filter prototype.

TABLE III
DIMENSIONS OF THE TUNABLE DUAL-MODE FILTER (IN MILLIMETERS)

l_{p1}	l_{p2}	$w_{p1,2}$	s	l_1
10.00	27.00	2.00	0.30	31.00
w_1	w_2	l_{g1}	l_d	w_d
4.00	6.00	9.60	1.40	1.70

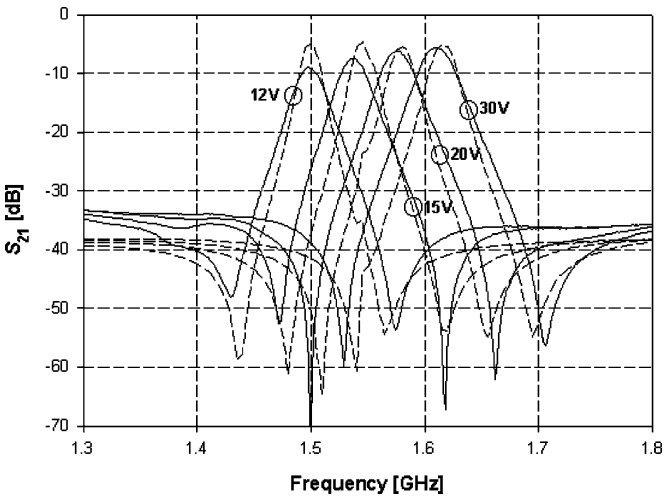

Fig. 19. Comparison of simulated and measured passband $|S_{21}|$ responses of varactor-tuned filter (– – –: simulated; ——: measured).

good dual-mode bandpass response is kept during the frequency tuning. When the applied tuning voltage is ranged from 12 to 30 V, the corresponding capacitance C_v of the varactor varies from 1.36 to 0.79 pF. The measured lower transmission zero relocates from 1.43 to 1.53 GHz, while the upper transmission zero changes from 1.57 to 1.71 GHz. As depicted in Fig. 19, the measured center frequency is tuned from 1.5 to 1.62 GHz and its 3-dB bandwidth in the tuning range is between 24–28 MHz. At a low bias voltage level, the contribution of the varactors to the

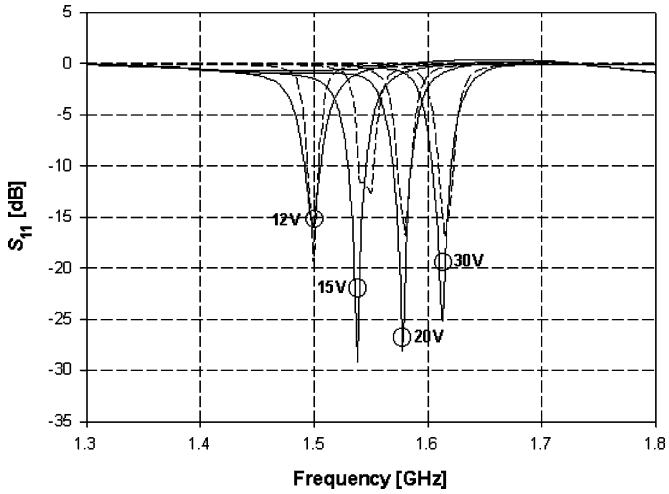

Fig. 20. Comparison of simulated and measured passband $|S_{11}|$ responses of varactor-tuned filter (– – –: simulated; ——: measured).

whole capacitance is greater and, therefore, the effects of losses (manifested through the diode and source series resistance) degrade the filter insertion loss performance. The return loss of this tunable filter is also recorded in Fig. 20, an overall good measured matching level of 20 to 30 dB is achieved in the above frequency tuning range.

V. Conclusion

In this paper, a novel microstrip square-loop dual-mode bandpass filter based on the CSIR has been presented. Its capabilities of spurious response suppression and size reduction have been thoroughly analyzed and discussed. A model has also been developed for accurate estimation of the passband response and the transmission zero locations. In addition, the insertion loss characterization has been derived. A compact prototype filter has been designed and experimentally characterized to demonstrate its usefulness. Besides, a varactor-tuned filter has been designed with a tuning range of 1.5–1.62 GHz. The measured results agree with the simulation, proving the tunable capability of this structure.

Acknowledgment

The authors would like to acknowledge the anonymous reviewers for their valuable comments and are also grateful to K.-F. Chang and W.-W. Choi, both with the University of Macau, Macao SAR, China, for technical discussions and support during the preparation of this paper.

References

[1] J. S. Hong and M. J. Lancaster, "Microstrip bandpass filter using degenerate modes of a novel meander loop resonator," *IEEE Microw. Guided Wave Lett.*, vol. 5, no. 11, pp. 371–372, Nov. 1995.

[2] P. Gardner and D. K. Paul, "Transmission line analysis of symmetrical ring resonators," *Proc. Inst. Elect. Eng.—Microw., Antennas, Propag.*, vol. 143, no. 2, pp. 184–188, Apr. 1996.

[3] L. Zhu and K. Wu, "A joint field/circuit model of line-to-ring coupling structures and its application to the design of microstrip dual-mode filters and ring resonators circuits," *IEEE Trans. Microw. Theory Tech.*, vol. 47, no. 10, pp. 1938–1948, Oct. 1999.

[4] L.-H. Hsieh and K. Chang, "Compact, low-insertion loss, sharp-rejection, and wideband microstrip bandpass filter," *IEEE Trans. Microw. Theory Tech.*, vol. 51, no. 4, pp. 1241–1246, Apr. 2003.

[5] A. Görür, "Description of coupling between degenerate modes of a dual-mode microstrip loop resonator using a novel perturbation arrangement and its dual-mode bandpass filter application," *IEEE Trans. Microw. Theory Tech.*, vol. 52, no. 2, pp. 671–677, Feb. 2004.

[6] J. Hong and M. J. Lancaster, "Theory and experiment of novel microstrip slow-wave open-loop resonator filters," *IEEE Trans. Microw. Theory Tech.*, vol. 45, no. 12, pp. 2358–2365, Dec. 1997.

[7] L. Zhu, P.-M. Wecowski, and K. Wu, "New planar dual-mode filter using cross-slotted patch resonator for simultaneous size and loss reduction," *IEEE Trans. Microw. Theory Tech.*, vol. 47, no. 5, pp. 650–654, May. 1999.

[8] A. Görür, C. Karpuz, and M. Akpinar, "A reduced-size dual-mode bandpass filter with capacitively loaded open-loop arms," *IEEE Microw. Wireless Compon. Lett.*, vol. 13, no. 9, pp. 385–387, Sep. 2003.

[9] K.-K. Sun and K.-W. Tam, "A novel compact dual-mode bandpass filter with meander open-loop arms," in *IEEE MTT-S Int. Microw. Symp. Dig.*, 2004, pp. 1479–1482.

[10] S. W. Fok, P. Cheong, K. W. Tam, and R. P. Martins, "Microstrip dual-mode bandpass filter design with simultaneous size reduction and spurious response suppression," in *IEEE MTT-S Int. Microw. Symp. Dig.*, 2005, pp. 2175–2178.

[11] M. Kirschning, R. H. Jansen, and N. H. L. Koster, "Measurement and computer-aided modeling of microstrip discontinuities by an improved resonator method," in *IEEE MTT-S Int. Microw. Symp. Dig.*, 1983, pp. 495–497.

[12] *"IE3D Manual,"* Zeland Software Inc., Fremont, CA, 2001.

[13] K. Chang, *Microwave Ring Circuits and Antennas*. New York: Wiley, 1996.

[14] G. L. Matthaei, L. Young, and E. M. T. Jones, *Microwave Filters, Impedance-Matching Networks, and Coupling Structures*. Norwood, MA: Artech House, 1980.

Si-Weng Fok (S'99) received the B.Sc. and M.Sc. degrees in electrical and electronics engineering from the University of Macau, Macao SAR, China, in 2003 and 2005, respectively.

Her research interests are RF/microwave passive structures and their application in active circuitry linearization.

Ms. Fok was the IEEE Student Branch Macau section secretary from 1999 to 2001 and treasurer from 2001 to 2002. She was the IEEE Microwave Theory and Techniques Society (IEEE MTT-S) Undergraduate Scholarship Recipient in 2002.

Pedro Cheong (S'98–M'03) received the B.Sc. and M.Sc. degrees in electrical and electronics engineering from the University of Macau, Macao SAR, China, in 2000 and 2005, respectively.

His research interests are mainly RF/microwave passive filter designs, modeling, and applications.

Kam-Weng Tam (S'91–M'01–SM'05) was born in Macau, China, in 1969. He received the joint Ph.D. degree in electrical and electronics engineering from the University of Macau, Macao SAR, China, and the Instituto Superior Técnico (IST), Technical University of Lisbon, Lisbon, Portugal, in 2000.

From 1993 to 1996, he was with the Instituto de Engenharia de Sistemas e Computadores (INESC), Lisbon, Portugal, where he participated in research and development on a broad range of applied microwave technologies for satellite communication system. Since 1996, he has been with the Electrical and Electronics Engineering, University of Macau, where he is currently an Associate Professor. From 1997 to 1999, he was on leave with the Instituto de Telecomunicações, Lisbon, Portugal, where he was involved in research and development on microwave filters, synthesizers, and phase-locked loops (PLLs). From July 2000 to December 2001, he was with the Instituto de Engenharia de Sistemas e Computadores (INESC), Macau, China, where he was Director involved with the development of communication and computer systems. From January 2002 to July 2003, he co-founded an analog and mixed-signal IP company in Macau, China, where he was the General Manager. His research interests are in the areas of microwave passive and active circuits and design of microwave microscopy for biomedical applications.

Prof. Tam helped in the formation of the IEEE Macau Section in 2003. He was the Technical Program co-chair of 5th IEEE Antennas and Propagation (AP)/Microwave Theory and Techniques (MTT) (HK-Macau) Postgraduate Conference. He supervised two IEEE Microwave Theory and Techniques Society (IEEE MTT-S) Undergraduate Scholarship Recipients in 2002 and 2003.

Rui P. Martins (M'88–SM'99) received the Licenciatura (Bachelor's), Master's, and Ph.D. degrees and the Agregação degree (Habilitation for full professor) in electrical engineering and computers from the Instituto Superior Técnico (IST), Technical University of Lisbon (UTL), Lisbon, Portugal, in 1980, 1985, 1992, and 2001, respectively.

Since October 1980, he has been an Academic Staff Member with the Electrical Engineering and Computers Department, IST/UTL. Since 1992, he has also been an Academic Staff Member with the Faculty of Science and Technology (FST), Electrical and Electronics Engineering Department, University of Macau, Macao SAR, China, on leave from IST, where he is a Visiting Full Professor since 1998. With the FST, he was the Dean of the Faculty from 1994 to 1997. He has been the Vice-Rector of the University of Macau since 1997. He has authored or coauthored over 100 scientific and academic works in the areas of microelectronics, electrical and electronics engineering, science, and education. His research interests include multirate signal processing and mixed analog/digital integrated-circuit design.

Dr. Martins was chairman of the IEEE Macau Section from 2004 to 2005. He is currently the chairman of the Joint Chapter of Circuits and Systems (CAS)/Communications (COMM). He was the recipient of the 1999 Medal of Professional Merit presented by the Macao Government (Portuguese Administration) and the 2001 Honorary Title of Value from the Macao SAR Government (Chinese Administration).